Journal of Natural Gas Science and Engineering 34 (2016) 873–885

Contents lists available at ScienceDirect

Journal of Natural Gas Science and Engineering

journal homepage: www.elsevier.com/locate/jngse

Syngas production from CO_2 reforming of methane over neodymium sesquioxide supported cobalt catalyst

Bamidele V. Ayodele [a, b], Sk Safdar Hossain [c], Su Shiung Lam [d], Osarieme U. Osazuwa [a, b], Maksudur R. Khan [a], Chin Kui Cheng [a, b, *]

[a] Faculty of Chemical & Natural Resources Engineering, Universiti Malaysia Pahang, Lebuhraya Tun Razak, 26300, Gambang Kuantan, Pahang, Malaysia
[b] Centre of Excellence in Advanced Research in Fluid Flow (CARIFF), Universiti Malaysia Pahang, Lebuhraya Tun Razak, 26300, Gambang Kuantan, Pahang, Malaysia
[c] Department of Chemical Engineering, King Faisal University, Al Hasa, Saudi Arabia
[d] Eastern Corridor Renewable Energy Group (ECRE), School of Ocean Engineering, Universiti Malaysia Terengganu, 21030, Kuala Terengganu, Terengganu, Malaysia

ARTICLE INFO

Article history:
Received 15 March 2016
Received in revised form
27 June 2016
Accepted 23 July 2016
Available online 26 July 2016

Keywords:
Cobalt
Dry reforming
Methane
Neodymium oxide
Syngas

ABSTRACT

This paper reports for the first time the catalytic dry (CO_2) reforming of methane over 20 wt%Co/80 wt% Nd_2O_3 catalyst. The catalyst was synthesized by wet-impregnation procedure and its physicochemical properties were characterized by TGA, XRD, FESEM, EDX, FTIR, H_2-TPR and TPD followed by activity testing in a fixed-bed reactor. The effects of feed ratios (CH_4: CO_2) ranged 0.1–1.0, reactant (CH_4 and CO_2) partial pressure (0–50 kPa) and temperature ranged 923–1023 K on the activity of the catalyst were investigated. The conversion of both reactants increased with the feed ratio and reaction temperature reaching maximum values of 62.7% and 82% for CH_4 and CO_2, respectively. The CO_2 reforming of methane resulted into the formation of syngas with maximum yields of 59.91% and 62.02% for H_2 and CO, respectively, leading to formation of syngas ratio of 0.97. The mechanistic proposition includes the CH_4 and CO_2 adsorption, activation of CH_4 by methane cracking and gasification of carbon deposited on the catalyst surface. The experimental data were fitted by Langmuir Hinshelwood kinetic models. Activation energy values of 21.89 and 62.04 kJ mol^{-1} were obtained for the consumption of CO_2 and CH_4 respectively from Langmuir-Hinshelwood models. The lower values of activation energy obtained for CO_2 compared to that of CH_4 shows that the rate of consumption of CO_2 was faster than that of CH_4 leading to higher conversion of CO_2.

1. Introduction

The sustainability of the energy derived from fossil sources has been a major subject of discussion by researchers in the last five decades (Ediger et al., 2007; Shafiee and Topal, 2009). The major concerns that have attracted wide attentions are the fast depletion in the world's fossil fuels reserve and the emission of greenhouse gases such as CO_2, CH_4 and N_2O into the environment from the utilization of energy derived from fossil fuels (Clarke et al., 2009; Shafiee and Topal, 2009). These have led to concerted efforts in searching for renewable and sustainable energy sources (Hashim and Ho, 2011). Renewable energy sources from biomass for the production of biofuels such as bioethanol, biodiesel and bio-jet fuels have been widely investigated (Rabelo et al., 2011; Ramírez-Verduzco, 2012; Timko et al., 2011). It is still however, debatable if biofuel can substitute the conventional fossil fuel in meeting the ever increasing global energy demand (Giampietro et al., 2006).

One way to simultaneously meet the global energy demand, as well as reduction in emission of these greenhouse gases is, via catalytic reforming process (Braga et al., 2014; Ross, 2005). The catalytic methane dry reforming can effectively mitigate the amount of greenhouse gases in the atmosphere which will invariably lead to the reduction in global warming (Djinović et al., 2012). Besides the advantage of reducing the emission of greenhouse gases, CH_4 which is one of the feedstock of the reforming process, constitutes about 95 mol % of natural gas (Union gas, 2015). Natural gas, although non-renewable, is inexpensive and abundant in

* Corresponding author. Faculty of Chemical & Natural Resources Engineering, Universiti Malaysia Pahang, Lebuhraya Tun Razak, 26300, Gambang Kuantan, Pahang, Malaysia.
E-mail address: chinkui@ump.edu.my (C.K. Cheng).

http://dx.doi.org/10.1016/j.jngse.2016.07.059
1875-5100/

nature with a proven world reserve of 187.1 trillion cubic metres (tcm) at the end of 2014 (British Petroleum, 2013). Natural gas as an essential commodity has been used as a major source of electricity generation, transportation fuel to power natural gas vehicles, as well as for domestic cooking and heating (Moore et al., 2014). However, the utilization of natural gas in all these processes contributes to emission of CO_2 (Shearer et al., 2014).

The methane dry reforming as in Equation (1) produces syngas, a mixture of carbon monoxide (CO) and hydrogen (H_2) which is suitable for the production of oxygenated fuels such as gasoline, biodiesels, and jet fuel via Fischer-Tropsch synthesis (Khodakov et al., 2007; Laosiripojana et al., 2005).

$$CH_4 + CO_2 \rightarrow 2H_2 + 2CO \quad \Delta H_{1023K} = 261 \text{ kJ mol}^{-1} \tag{1}$$

Besides the main reaction (cf. Equation (1)), the methane cracking, Boudouard reaction, reverse water gas shift reaction, reduction of CO_2 and reduction of CO as in Equations (2)–(6), respectively, are the other side reactions commonly occur during the methane dry reforming (Lavoie, 2014) that unfortunately yielded carbon deposit (Han et al., 2013; Serrano-Lotina and Daza, 2014).

$$\mathrm{CH_4} \leftrightarrow \mathrm{C} + 2\mathrm{H_2} \quad \Delta\mathrm{H_{298K}} = +74.9 \text{ kJ mol}^{-1} \tag{2}$$

$$2\mathrm{CO} \leftrightarrow \mathrm{C} + \mathrm{CO_2} \quad \Delta\mathrm{H_{298K}} = -172.4 \text{ kJ mol}^{-1} \tag{3}$$

$$\mathrm{CO_2} + 2\mathrm{H_2} \leftrightarrow \mathrm{C} + 2\mathrm{H_2O} \quad \Delta\mathrm{H_{298K}} = -90 \text{ kJ mol}^{-1} \tag{4}$$

$$2\mathrm{H_2} + 2\mathrm{CO} \leftrightarrow 2\mathrm{H_2O} + 2\mathrm{C} \quad \Delta\mathrm{H_{298K}} = -131.3 \text{ kJ mol}^{-1} \tag{5}$$

$$\mathrm{CO_2} + \mathrm{H_2} \leftrightarrow \mathrm{CO} + \mathrm{H_2O} \quad \Delta\mathrm{H_{298K}} = +37.67 \text{ kJ mol}^{-1} \tag{6}$$

Studies showed that carbon deposition is one of the major causes of catalyst deactivation in methane dry reforming in addition to the sintering and poisoning effects (Lakhapatri and Abraham, 2009; Nair et al., 2014). There have been a lot of attentions on synthesizing catalysts that are thermally stable and less prone to deactivation by carbon deposition (Sato and Fujimoto, 2007; Tungkamani and Phongaksorn, 2013; Zhang et al., 2007). To date, noble metals/transition metals such as Pd, Pt, Ru, Rh, Ni and Co dispersed on supports, i.e. Al_2O_3, MgO, CeO_2, La_2O_3, ZrO_2, SBA-15 and SiO_2 have been investigated for methane dry reforming (El Hassan et al., 2016; Abasaeed et al., 2015; Ba et al., 2014; Bouarab et al., 2004; Itkulova et al., 2005; Mattos et al., 2003; Sokolov et al., 2013; Ocsachoque et al., 2011). Previous studies have shown that the use of rare earth metals oxides such as CeO_2 and La_2O_3 as supports for metal-based catalysts enhance the catalytic activities and stability (Ayodele et al., 2015a; Verykios, 2003). The enhanced performance of these rare earth metal oxides supported metal-based catalysts is due to their basic surface characteristic as well as high oxygen storage-release capacity (Sato et al., 2009; Zhang et al., 2006). Although extensive studies have been done on the use of rare earth metal oxides such as CeO_2 for synthesis of Co-based catalyst in methane dry reforming, to the best of our knowledge, literature on the catalytic performance of Nd_2O_3 supported Co catalyst for the methane dry reforming has not been reported. Therefore, the present study focuses on the synthesis, characterization and catalytic performance of 20 wt%Co/80 wt% Nd_2O_3 catalyst for application in methane dry reforming. The application of Nd_2O_3 as support for the dispersion of Co, is based on its advantages as reported by (Sato et al., 2009). According to Sato et al. (2009), the surface characteristic of Nd_2O_3 is basic rather than acidic. This implies that the synthesis of Co on the Nd_2O_3 will enhance the activation of CO_2 during the methane dry reforming reaction since CO_2 is an acidic gas. Moreover, Nd_2O_3 as a rare earth metal oxide has a high oxygen storage-release capacity. During methane dry reforming valence oxygen can be released from the Nd_2O_3 for gasification of deposited coke on the catalysts surface. The choice of 20 wt% Co-loading used in this study was based on the findings of Budiman et al. (2016), Jacobs et al. (2002) and Ma et al. (2004) who investigated the effect of Co loading (2 wt%–35 wt%) on the catalytic performance of supported Co catalysts. The authors concluded that the catalyst with 20 wt% Co-loading had better performance compare to those with lower Co-loadings (<20 wt%).

2. Experimental

2.1. Synthesis of 20 wt%Co/80 wt%Nd_2O_3 catalyst

Prior to the catalyst synthesis, the Nd_2O_3 powder was obtained from thermal decomposition procedure, in accordance with reported literature (Ayodele et al., 2016a; Hussein, 1996; Kępiński et al., 2004). The Nd_2O_3 precursor, $Nd(NO_3)_3.6H_2O$ (99.9% trace metal basis, Sigma-Aldrich) was heated under the air flow at 773 K for 2 h, to obtain Nd_2O_3 powder. The Nd_2O_3 powder was subsequently crushed to obtain required particle size suitable for the synthesis of the Co-catalyst. For the preparation of the 20 wt%Co/80 wt%Nd_2O_3 catalyst, 15.52 g of $Co(NO_3)_2.6H_2O$ (99.99% trace metal basis, Sigma-Aldrich) equivalent to 20 wt% Co loading were dissolved in 20 ml distilled water. The aqueous solution was subsequently impregnated into 20 g of the Nd_2O_3 powder to obtain the catalyst slurry. The slurry was continuously stirred for 3 h, followed by drying at 393 K for 24 h and calcination under air flow at 873 K for 5 h.

2.2. Characterization of catalyst

Several techniques such as thermogravimetric analysis (TGA), X-ray powder diffraction (XRD), field emission scanning electron microscopy (FESEM), energy dispersive X-ray spectroscopy (EDX), N_2 adsorption-desorption analysis, temperature programmed reduction (H_2-TPR) temperature programmed desorption (TPD), and Fourier transform infra-red spectroscopy (FTIR) were employed for characterization of the as-synthesized 20 wt%Co/80 wt%Nd_2O_3. The weight changes of uncalcined, fresh catalyst as a function of temperature was performed by a TGA instrument (TA instruments, Q500). The thermogravimetric (TG) and the differential thermogravimetric (DTG) profiles representing the non-isothermal catalyst weight loss and derivative weight loss, respectively, were measured over temperatures that ranged from 298 to 1273 K employing heating rates of 10, 15 and 20 K min^{-1}, respectively, in a flow of compressed air. The activation energy of the decomposition of dried fresh catalyst ($Co(NO_3)_2/Nd_2O_3$) was evaluated using Kissinger equation as in (7) (Blaine and Kissinger, 2012).

$$\ln\left[\frac{\beta}{T_m^2}\right] = \ln\left[\frac{ZR}{E}\right] - \frac{E}{RT_m} \tag{7}$$

where β, T_m, R, Z and E are the heating rate, peak temperature, universal gas constant, Arrhenius pre-exponential factor and activation energy, respectively. Carbon deposited on the spent catalyst was analysed by temperature programmed oxidation (TPO) under compressed air atmosphere (20% O_2 and 80% N_2, total flow = 50 ml/min) using the same TA Q500 series instrument.

The crystalline phase of the calcined catalyst was determined by

Rigaku X-ray powder diffraction instrument (Miniflex II) operating at 600 W (X-ray tube, CuKα with $\lambda = 0.154$ nm). The diffraction peaks were measured in the 2θ ranged 10°–80° by PDXL full-function powder diffraction analysis package. The surface morphology of the fresh catalyst was obtained by FESEM (JEOL, JSM-7800F) equipped with Schottky-type field-emission electron source while the elemental composition was measured by EDX. The textural properties were obtained from the N_2 adsorption-desorption analysis using Thermo Scientific Surfer Analyzer. Prior to the analysis, the catalyst sample was degassed at 523 K for 4 h and the N_2 adsorption-desorption measured at 77 K. The reducibility of the catalyst was measured by H_2-temperature programmed reduction (H_2-TPR) using Thermo-Scientific TPDRO 1100 apparatus equipped with TCD detector. Approximately 60 mg of the catalyst sample was initially pre-treated in a flow of 20 ml min^{-1} N_2 at heating rate of 10 K min^{-1} up to 393 K at holding period of 30 min. Subsequently, the pre-treated catalyst sample was reduced with 20 ml min^{-1} of 5% H_2 in N_2 carrier gas at heating rate of 10 K min^{-1} up to 1173 K with holding period of 60 min before cooling to room temperature In addition, the acidity and basicity of the catalytic surface were evaluated in a Thermo Finnigan TPDRO 1100, using NH_3 and CO_2 probe molecules, respectively. The FTIR spectrum of the catalyst sample was collected at room temperature using Thermo Scientific FTIR (Nicolet iS-50) in wavenumber ranged 4000–400 cm^{-1}. The sample was prepared for spectra collection by mixing a proportion of 1:10 of solid sample: KBr. The catalyst sample and the KBr were ground beforehand to reduce the particle. The sample mixture was then pressed into a pellet using Qwik Hand-Press for 2 min. The IR spectrum was collected over the KBr pellet at a resolution of 4 cm^{-1} and 16 scanning.

2.3. Catalytic activity evaluation

The catalytic methane dry reforming over 20 wt%Co/80 wt% Nd_2O_3 catalyst was performed in a laboratory-scale fixed bed stainless steel reactor as depicted in Fig. 1. The fixed-bed tubular reactor (ID: 10 mm and length: 35 cm) containing 200 mg weight of 20 wt%Co/80 wt%Nd_2O_3 catalyst was vertically positioned in a split-tube furnace. The temperature of the catalyst bed was monitored using a type-K thermocouple. The catalyst was reduced *in-situ* in a flow of 60 ml min^{-1} of H_2/N_2 (1:5) for 1 h, followed by purging with 50 ml/min of N_2 flow for 20 min before the commencement of reaction study. The activity was investigated at temperatures that ranged 923–1023 K and CH_4:CO_2 from 0.1 to unity (sub-stoichiometric to stoichiometric ratios). All the gas flows were monitored by Alicat digital mass flow controllers, with the overall gas hourly space velocity (GHSV) fixed at 30 000 h^{-1}. The compositions of the products (CO and H_2) as well as that of the reactants (CH_4 and CO_2) were measured by a gas chromatography instrument (Agilent GC system 6890 N Series) equipped with thermal conductivity detector (TCD). The GC system consists of two packed columns, namely Supelco Molecular Sieve 13 × (10 ft × 1/8 in OD × 2 mm ID, 60/80 mesh, Stainless Steel) and Agilent Hayesep DB (30 ft × 1/8 in OD × 2 mm ID, 100/120 mesh, Stainless Steel). Helium gas with a flowrate of 20 ml min^{-1} was used as the carrier gas at the operating column temperature of 393 K. The catalytic performance of the methane dry reforming was evaluated in terms of:

$$CH_4\ \text{conversion}\ (\%) = \frac{F_{CH_{4in}} - F_{CH_{4out}}}{F_{CH_{4in}}} \times 100 \tag{8}$$

$$CO_2\ \text{conversion}\ (\%) = \frac{F_{CO_{2in}} - F_{CO_{2out}}}{F_{CO_{2in}}} \times 100 \tag{9}$$

$$\text{Syngas ratio}\ \frac{H_2}{CO} = \frac{\text{mole of } H_2 \text{ produced}}{\text{mole of CO produced}} \tag{10}$$

$$H_2\ \text{yield} = \frac{F_{H_{2out}}}{2 \times F_{CH_{4in}}} \times 100 \tag{11}$$

$$\text{CO yield} = \frac{F_{CO_{out}}}{F_{CH_{4in}} + F_{CO_{2in}}} \times 100 \tag{12}$$

where by $F_{CO_{2in,}}$ = inlet molar flow of CO_2;$F_{CO_{2out}}$ = outlet molar flow of CO_2;$F_{CH_{4in,}}$ = inlet molar flow of CH_4;$F_{CH_{4out}}$ = outlet molar flow of CH_4.

3. Results and discussion

3.1. Catalyst characterization

The temperature programmed calcination profile showing the weight loss and derivative weight of the fresh, uncalcined catalyst is shown in Fig. 2. Four different peaks (I–IV) corresponding to the sequential loss of hydrated water (peaks I–III) and the decomposition of the cobalt nitrate salt to its oxide (Co_3O_4) (peak IV) can be identified from the profiles and described in Equations (13)–(16).

$$\text{(I)}\quad Co(NO_3)_2 \cdot 6H_2O \rightarrow Co(NO_3)_2 \cdot 4H_2O + 2H_2O \tag{13}$$

$$\text{(II)}\quad Co(NO_3)_2 \cdot 4H_2O \rightarrow Co(NO_3)_2 \cdot 2H_2O + 2H_2O \tag{14}$$

$$\text{(III)}\quad Co(NO_3)_2 \cdot 2H_2O \rightarrow Co(NO_3)_2 + 2H_2O \tag{15}$$

$$\text{(IV)}\quad Co(NO_3)_2 \rightarrow CoO + N_2O_5 \text{ followed by } 3CoO + \tfrac{1}{2}O_2 \rightarrow Co_3O_4 \tag{16}$$

This trend is consistent with the findings of Foo et al. (2011) who used cobalt (II) nitrate hexahydrate as a precursor for the preparation of their supported Co catalysts. The activation energy values associated with the loss of hydrated water as well as thermal decomposition of the cobalt nitrate salt were estimated from Kissinger plots as depicted in Fig. 3 and further summarized in Table 1. It can be seen that the activation energy increased from 70.84 to 130.20 kJ mol^{-1} with decrease in hydration water. This trend has been reported by Ihli et al (Ihli et al., 2014). whereby it was suggested that the removal of OH bond during calcination is responsible for the increase in the activation energy. The highest activation energy of 262.32 kJ mol^{-1} was obtained for the two-steps Co_3O_4 formation (cf. Equation (16)).

The XRD pattern of the fresh and reduced calcined 20 wt%Co/80 wt% Nd_2O_3 catalyst shown in Fig. 4 matches well with the XRD data of Co (ICDD card No 00-001-1254), Co_3O_4 (ICDD card No 00-009-0418), Nd_2O_3 (ICDD card No 00-006-0408) and $NdCoO_3$ (ICDD card No 00-025-1064). Significantly, the diffraction peaks of the fresh calcined 20 wt%Co/80 wt% Nd_2O_3 catalyst at 2θ of 23.75° (200), 27.12° (100), 38.70° (222), 41.59° (101), 44.85° (400), and 70.59° (220) can be assigned to the spinel cubic phase of Co_3O_4 (Fakeeha et al., 2014) while the diffraction peaks at 2θ of 37.18° (210), 44.85° (102), 49.97° (410), and 65.35° (202), correspond to the hexagonal phase of Nd_2O_3 (Kępiński et al., 2004). The formation cubic structure of Perovskite $NdCoO_3$ from the interaction between Co_3O_4 and Nd_2O_3 is evident at 2θ = 33.70°(220), 37.03°(311), 48.38°(400), 60.10°(422). Interestingly, the XRD of the reduced catalyst (cf. Fig. 4) confirmed the complete reduction of all the Co containing species (perovskite $NdCoO_3$ and Co_3O_4) under the flow

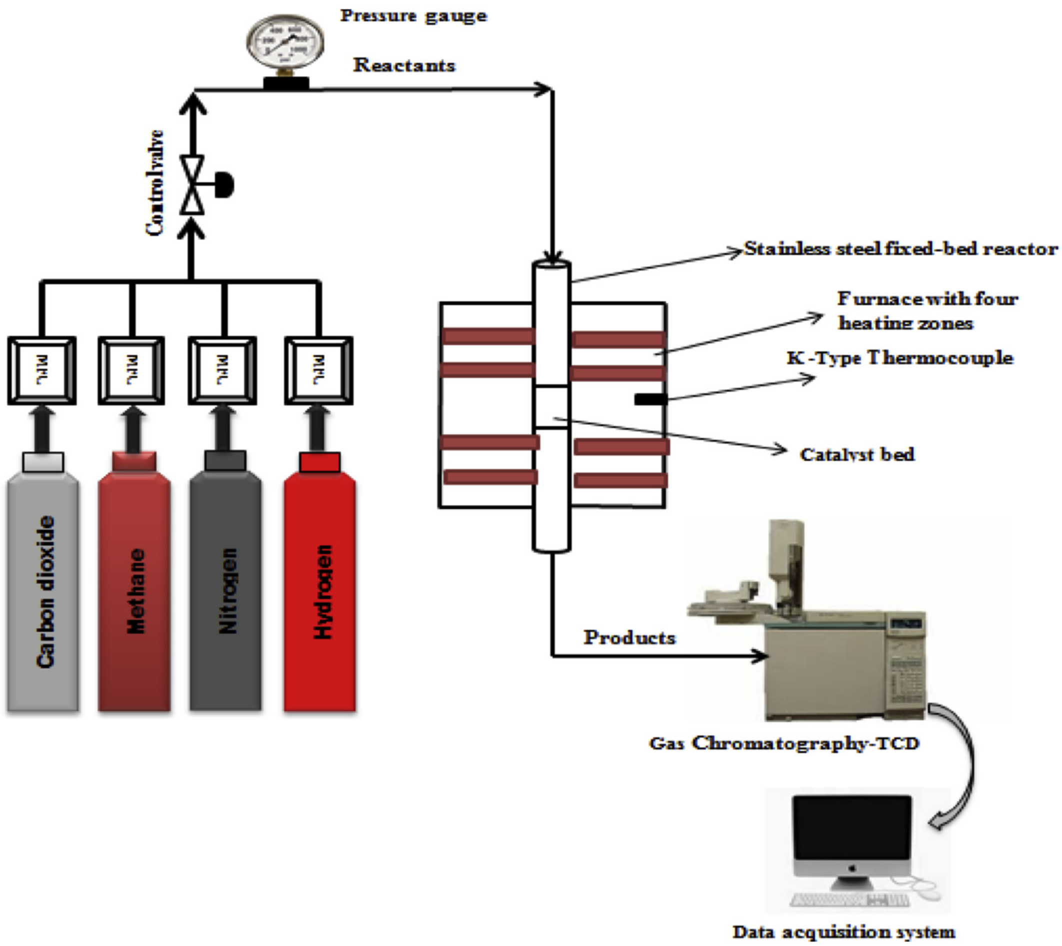

Fig. 1. Schematic representation of the experimental set up used for the methane dry reforming over 20 wt%Co/80 wt%Nd_2O_3.

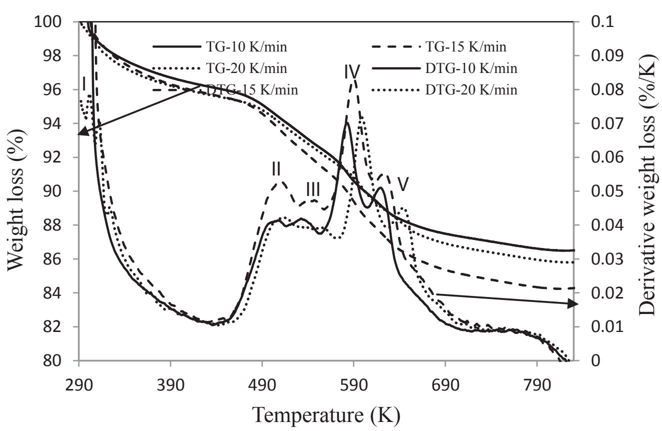

Fig. 2. Temperature Programmed Calcination profile of the 20 wt% Co/80 wt%Nd_2O_3 catalyst.

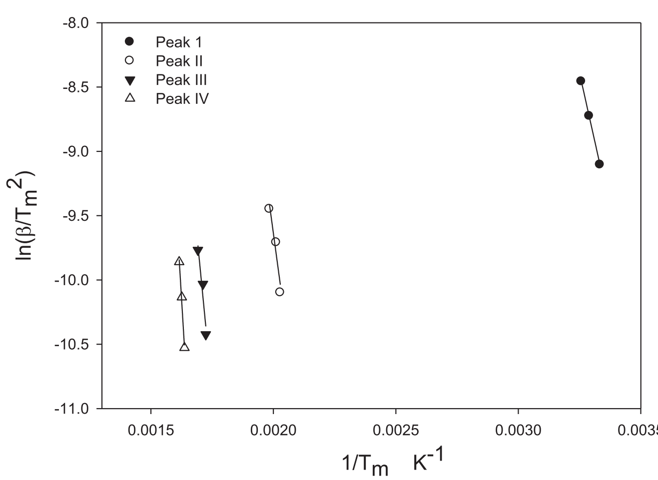

Fig. 3. Evaluation of activation energy from the linearized Kissinger model.

of H_2 during activation, to crystallite Co° prior to the commencement of the methane dry reforming reaction which is consistent with the H_2-TPR profile showing two reduction peaks which corresponds to the H_2-reduction of $NdCoO_3$ and Co_3O_4. The Nd_2O_3 crystal size with full-width at half maximum diffraction (FWHM) peak ($2\theta = 33.74$) of the fresh calcined 20 wt%Co/80 wt% Nd_2O_3 catalyst was estimated as 27.5 nm using the Scherrer Equation as in (17):

$$d = \frac{0.94\lambda}{\beta\cos\theta} \tag{17}$$

where d, β, θ, and λ are the crystallite size, full-width at half maximum (FWHM) of the diffraction peak, half of the diffraction angle and radiation wavelength, respectively.

Similarly, the particle size of the Co° ($2\theta = 22.23°$) and Nd_2O_3

Table 1
Activation energy for the calcination of fresh, dried 20 wt%Co/80 wt%Nd_2O_3 catalyst.

Peak	E_a (kJ mol^{-1})	R^2
I	70.84	0.99
II	117.07	0.93
III	130.20	0.93
IV	262.32	0.99

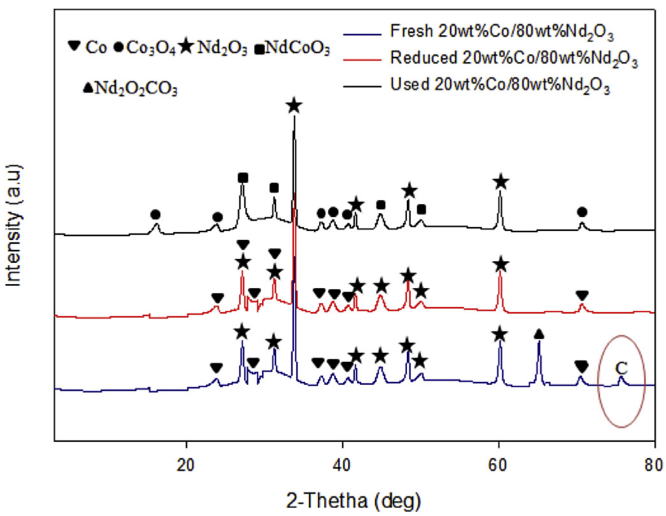

Fig. 4. XRD pattern of the fresh, reduced and used 20 wt%Co/80 wt%Nd_2O_3 catalysts.

crystals of the used catalyst was estimated as 8.77 nm and 27.7 nm, respectively. This indicates that catalyst sintering was avoided during the methane dry reforming, a testament of thermal stability property of the 20 wt%Co/80 wt%Nd_2O_3.

The morphology and elemental composition of the Nd_2O_3 supported Co catalyst are depicted in the FESEM micrographs, EDX micrograph and dot-mapping shown in Fig. 5. The irregular shapes and the agglomerated particles are most likely belongs to the Co metal that has been uniformly-distributed on the surface of the Nd_2O_3 which appeared as flat slabs (Fig. 5(a) and (b)). The EDX micrograph of the catalyst confirms the presence of Co (17.25%), Nd (58.92%) and O (24.83%) (cf. Fig. 5(c)). The elemental composition obtained from the EDX micrograph relatively corresponds to distribution shown in the dot mapping (Fig. 5(d)) and the stipulated amount in the as-synthesized 20 wt%Co/80 wt%Nd_2O_3 catalyst.

In addition, the textural property of the fresh 20 wt%Co/80 wt% Nd_2O_3 catalyst was determined from N_2 physisorption analysis. The resulting N_2 adsorption-desorption isotherm is shown in Fig. 6, whereby it displays a type-V IUPAC classification signifying multilayer adsorption (Donohue and Aranovich, 1998). It is noteworthy that the adsorption process was accompanied by capillary condensation. This is evident from the point of interception of the type H3 hysteresis which is at relative pressure <0.6. The textural analysis of the catalyst yielded BET specific surface area, average pore diameter and pore volume of 18.67 m^2 g^{-1}, 1.19 nm and 0.0061 cm^3 g^{-1}, respectively. A separately carried out analysis (isotherm not shown) for the pristine Nd_2O_3 support gave a BET specific surface of 6.76 m^2 g^{-1}. The larger BET specific surface area obtained for the 20 wt%Co/80 wt%Nd_2O_3 catalyst can be attributed to the dispersion of the cobalt catalyst on the Nd_2O_3 support. Most likely, the dispersion of the Co metal on the support has resulted in the formation of more fine particles on the Nd_2O_3 support (cf. Fig. 5) resulting in an attainment of higher BET specific surface area.

The H_2-TPR profile showing the reducibility of the freshly calcined 20 wt%Co/80 wt%Nd_2O_3 catalyst is depicted in Fig. 7. Interestingly the TPR curves of the Co-impregnated catalyst displayed major reduction peaks cantered at 673 K and 825 K. These peaks are indication of different degree of Co–Nd_2O_3 interaction. Based on the XRD pattern (cf. Fig. 4) of the 20 wt%Co/80 wt%Nd_2O_3 catalyst, Co_3O_4, and $NdCoO_3$ have been identified for H_2-reduction. The low temperature reduction peak at 673 K could be attributed to the H_2-reduction of the Co_3O_4 phase to Co° and the peak cantered at 825 K correspond to the H_2-reduction of $NdCoO_3$ as shown in Equations (18) and (19) (Choudhary and Mondal, 2006).

$$Co_3O_4 + 4H_2 \rightarrow 3Co^o + 4H_2O \quad (18)$$

$$2NdCoO_3 + 3H_2 \rightarrow 2Co^o + Nd_2O_3 + 3H_2O \quad (19)$$

The strength of the acid and basic site of the 20 wt%Co/80 wt% Nd_2O_3 catalyst was also measured by the means of TPD using CO_2 and NH_3 as probe gases. The degree of acidity or basicity of the catalyst sites is usually measured as a function of temperature range where the chemisorbed probed gases (CO_2 and NH_3) would be desorbed. The desorption of a probe gas at lower temperature range signifies weak basic site while desorption at a higher temperature range implies strong site. The CO_2- and NH_3-TPD profiles for the as-synthesized catalyst are shown in Fig. 8(a) and (b), respectively. Interestingly, the 20 wt%Co/80 wt%Nd_2O_3 catalyst has both acid and basic sites. Two distinct desorption peaks at 950 and 1040 K, respectively, can be observed from the NH_3-TPD profile indicating the presence of strong acid site. Similarly, the CO_2-TPD profile shows two superimposed peaks at 900 and 1180 K, respectively, and a big peak at 980 K signifying the presence of medium and strong basic site. The estimation of the overall amount of CO_2 and NH_3 adsorbed has yielded 427.39 μmol g^{-1} for basic site compared to 165.87 μmol g^{-1} for the acid site, indicating that the catalyst possessed a net-basic property.

3.2. Catalytic methane dry reforming evaluation

The effects of feed ratios (0.1–1.0) and reaction temperature (923–1023 K) on the conversions of CH_4 and CO_2 to syngas over 20 wt%Co/80 wt%Nd_2O_3 catalyst was investigated. Significantly, the conversions of both the CH_4 and CO_2 increased non-linearly with the feed ratios (cf. Fig. 9). At 1023 K, the conversion of CH_4 increased from 12.8% at CH_4:CO_2 of 0.1–62.7% at CH_4:CO_2 ratio of unity, while in the similar CH_4:CO_2 range, the conversion of CO_2 jumped from 50% to circa 80%. Since the conversions recorded by both CH_4 and CO_2 were not similar, as opposed to their proposed methane dry reforming reaction (refers to Equation (1)), we posit that the CH_4 may exhibit poorer affinity to the catalyst, most likely due to the presence of stronger basic sites that favoured CO_2 adsorption as indicated by the TPD results (Pakhare et al., 2014; Sato et al., 2009). Indeed, the conversion of CH_4 was always lower than its counterpart (CO_2), further lending credence to our current proposition. Our current finding is comparable with the findings from Ayodele et al. (2015b), Budiman et al. (2016), Djinović et al. (2012), El Hassan et al. (2016) and Jabbour et al. (2014) who investigated methane dry reforming over 20 wt%Co/CeO_2, 20 wt%Co/SiO_2, 2 wt%Rh/CeO_2 12 wt%Co/SiO_2, 12 wt%Co/SBA-15 and 12wtCo/SBA-15 catalysts respectively. The authors findings showed that CO_2 conversions of 87.6%, 22%, 25%, 80%, 70% and 44% were obtained using 20 wt%Co/CeO_2, 20 wt%Co/SiO_2, 2 wt%Rh/CeO_2 12 wt%Co/SiO_2, 12 wt%Co/SBA-15 and 12wtCo/SBA-15 catalysts respectively compared to the 80% CO_2 conversion obtained in this study. Furthermore, CH_4 conversions of 79.5%, 45%, 98%, 80%, 25% and 40% were obtained using 20 wt%Co/CeO_2, 20 wt%Co/SiO_2, 2 wt%Rh/CeO_2 12 wt%Co/SiO_2,

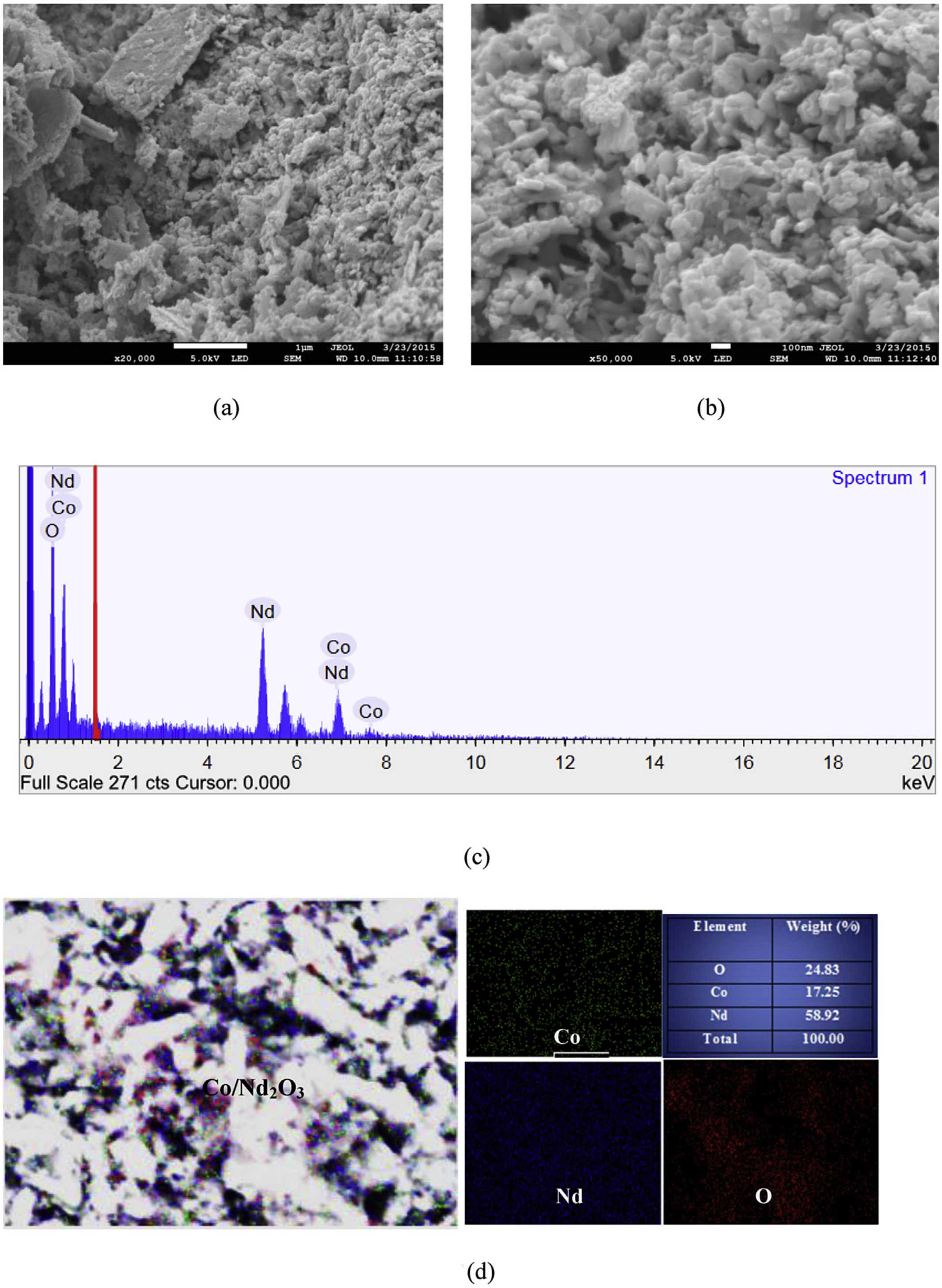

Fig. 5. FESEM micrographs at (a) ×20000, (b) ×50000 and (c) EDX micrograph (d) EDX dot mapping for the fresh 20 wt%Co/80 wt%Nd_2O_3 catalyst.

12 wt%Co/SBA-15 and 12wtCo/SBA-15 catalysts respectively compared to the 62.7% CH_4 conversion obtained in this study. The variation in the catalytic performance could be due to the differences in the extent of dispersion of the active phase on the supports which is a function of the preparation methods. In addition, these variations in the catalytic performance could also be attributed to the differences in the catalysts physicochemical properties such as BET specific surface area, the pore volumes, reducibility and the surface acidity/basicity. It is also noteworthy that conversion increased with the reaction temperature, in accordance to the Arrhenius trend (Peleg et al., 2012). In addition, the excess CO_2 scenario compelled it to partake in reactions such as the reverse-Boudouard (reverse of Equation (3)) and also reverse-water gas shift, consequently higher CO_2 conversion (Acharya et al., 2013; Haag et al., 2007).

The yields of H_2 and CO, the main component of syngas, are depicted in Fig. 10. It can be seen that the syngas yield increased significantly with feed ratios and temperature, from 15.68% to

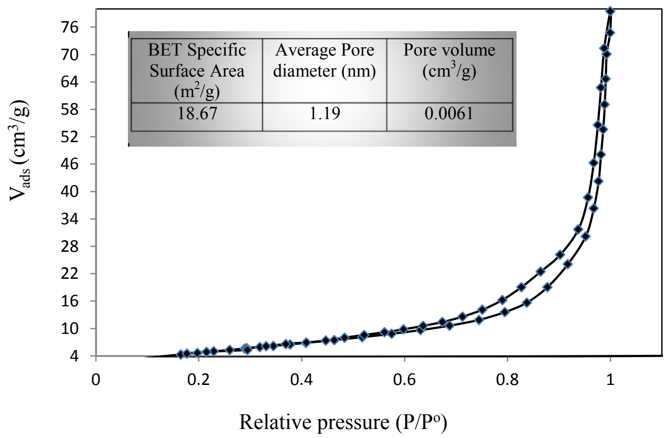

Fig. 6. N_2 adsorption-desorption isotherm for the fresh 20 wt%Co/80 wt%Nd_2O_3 catalyst.

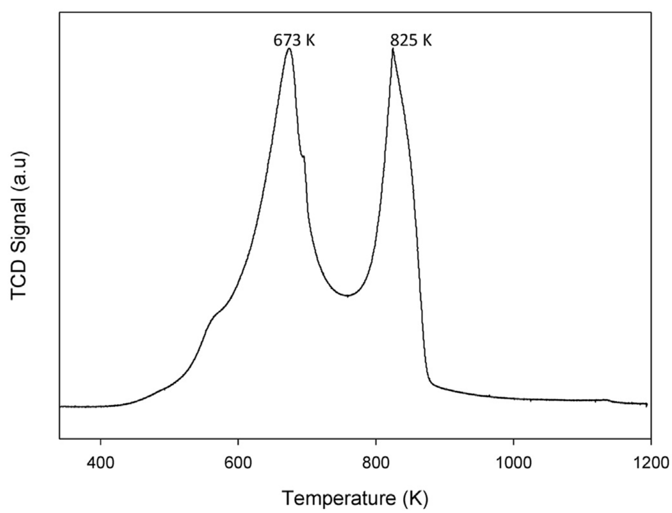

Fig. 7. H_2-TPR profile of 20 wt%Co/80 wt%Nd_2O_3.

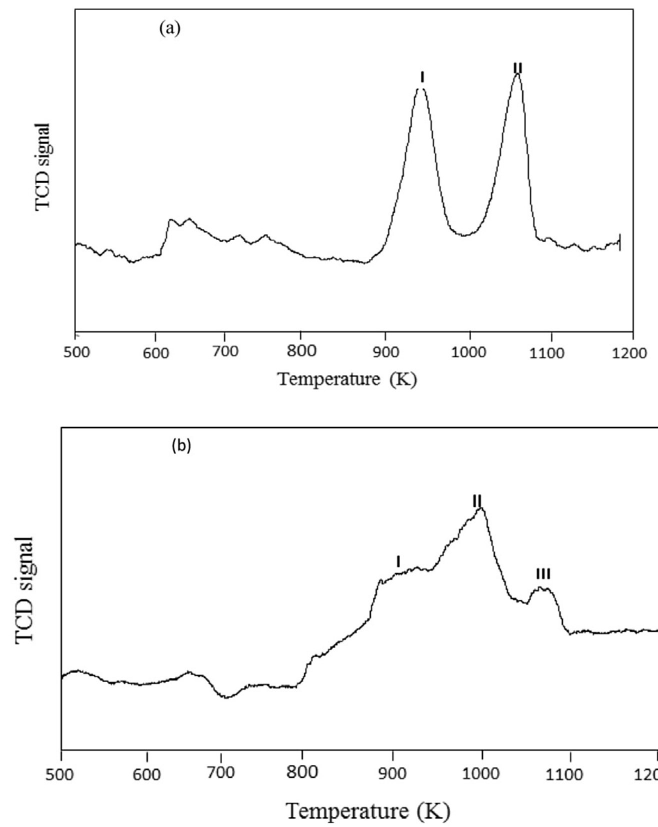

Fig. 8. Temperature programmed desorption profile of 20 wt%Co/80 wt%Nd_2O_3 using (a) NH_3 and (b) CO_2 as probe gases.

27.40%, to 59.91% and 62.78%, respectively, at reaction temperature of 1023 K, in tandem with the conversion trend exhibited by the reactants. Once again, similar trend was portrayed by reactions that were carried out at 973 and 923 K. However, the H_2 and CO yields are higher compared to that obtained by Ruckenstein and Wang (2000) and Takanabe et al. (2005). The highest yield of 31.9% and 46.3% were obtained for H_2 and CO, respectively, by Ruckenstein & Wang at 1073 K while Sajjadi et al. (2014) reported 8.8% and 28.8% for H_2 and CO, respectively, using 12 wt%Co/CaO and 0.5 wt%Co/TiO catalysts. The noticeable difference could be as result of difference in reaction temperatures as well as the catalyst loadings. Interestingly, the highest values of the H_2 and CO yields which was obtained at the feed ratio of 1.0 and temperature of 1023 K translates to syngas ratio of 0.97. This makes the syngas produced suitable as feedstock for synthesis fuel production via FTS (Botes et al., 2013). The syngas ratio of 0.97 obtained from the present study is consistent with 0.98 obtained by Nematollahi et al. (2011). This slight difference could be as result of influence of both reverse water gas shift reaction which reduces the amount of H_2 formed and/or loss of CO through the reaction H_2 formed from methane decompositions.

3.3. Thermodynamic and equilibrium conversion

In order to measure the limit for CH_4 and CO_2 conversion as a function of changes in temperature, a thermodynamic equilibrium analysis was performed at total pressure of 101.3 kPa, CH_4:CO_2 ratio 1:1 (N_2 was used as a diluent) and temperature ranged 573–1273 K. Fig. 11 shows the equilibrium conversions of CH_4 and CO_2 obtained as a function of temperature. Interestingly, the equilibrium conversion increases with increase in temperature. From Fig. 11 the equilibrium conversions of 45.01%, 50.63% and 72.4% were obtained at reaction temperature of 923, 973, and 1023 K respectively for CH_4 while equilibrium conversions of 62.45%, 75.67% and 88.56% at reaction temperature of 923, 973, and 1023 K respectively were obtained for CO_2. In order to minimize the influence of methane cracking (which is often responsible for the release of coke that leads to deactivation) on the kinetic measurement, the CH_4:CO_2:N_2 flow rate were adjusted to keep the conversion of CH_4 distant from the thermodynamic equilibrium.

3.4. Effect of mass and heat transfer

In order to determine suitable conditions under which the effect of external mass transfer are negligible, a preliminary runs was performed by varying the total CH_4:CO_2:N_2 flow rate from 20 to 200 ml min^{-1} at 1023 K. The effect of the total feed rate on CH_4 conversion is depicted in Fig. 12. It can be seen from Fig. 12 that the CH_4 conversion is dependent on the total gas feed rate between 20 and 80 ml min^{-1}. At gas flow rate >90 ml min^{-1}, the conversion of CH_4 was found to be independent of the gas flow rate. Hence, it can be assumed that the influence of external mass transfer on the kinetic measurement is negligible at gas flow rate >90 ml min^{-1}.

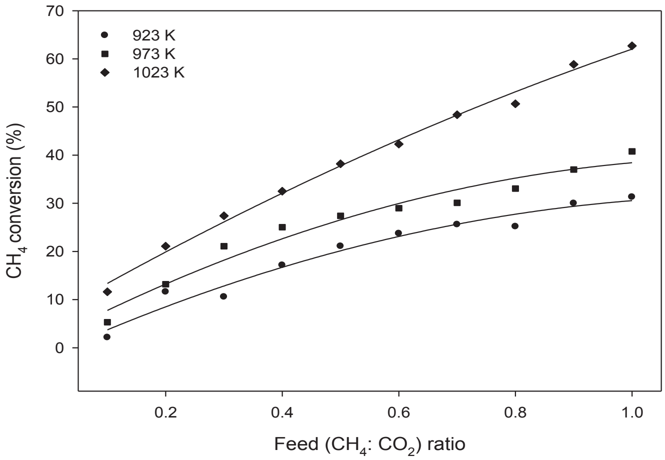

(a)

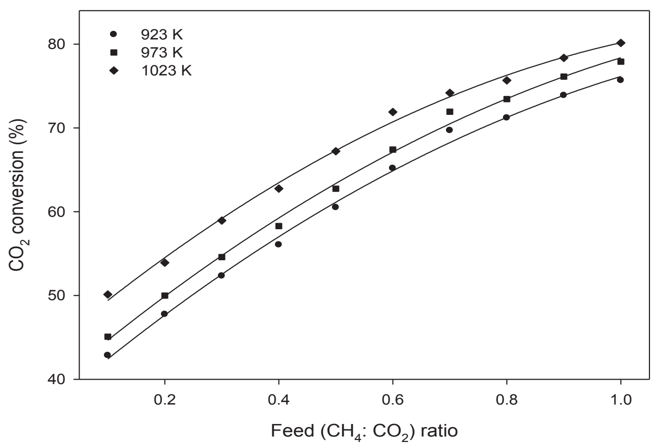

(b)

Fig. 9. Conversion of (a) CH_4 and (b) CO_2 from methane dry reforming over 20 wt%Co/80 wt%Nd_2O_3 catalyst.

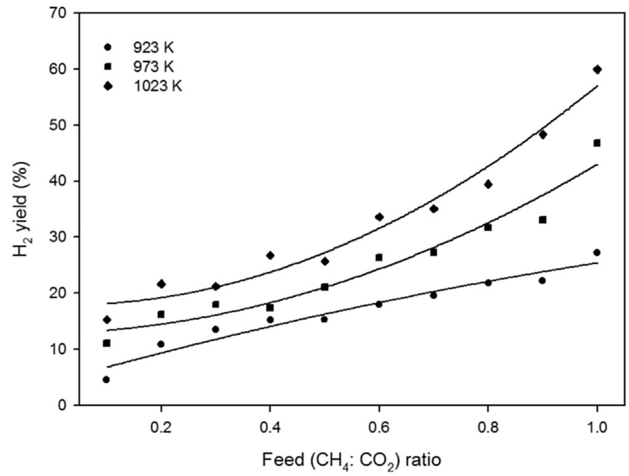

(a)

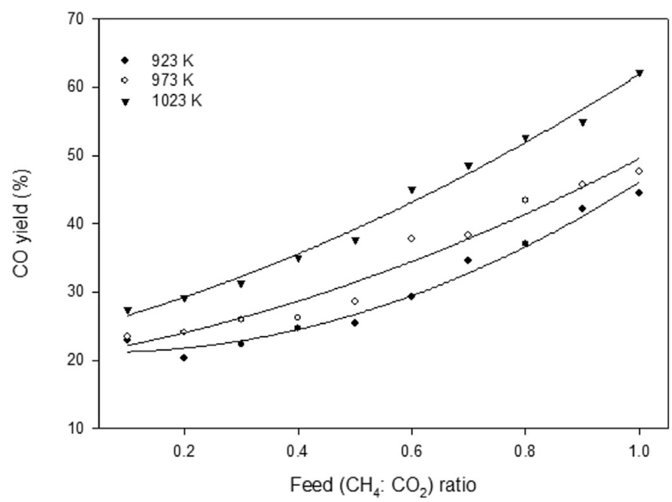

(b)

Fig. 10. Yields of (a) H_2 and (b) CO, as a function of feed ratios and temperatures.

This justifies the choice of using GHSV of 30000 h^{-1} which was estimated based on the total gas flow rate of 100 ml min^{-1}.

To further investigate the effect of gaseous-solid heat- and mass-transfer limitations on the methane dry reforming reaction over the catalyst, the Mear's and Weisz-Prater criteria (Mears, 1971; Weisz and Prater, 1954) criteria which are based on the assumption that the catalyst's particles are spherical were employed. Based on the Mears criterion the impact of external heat intrusion on the reaction rate can be assumed negligible if the relationship in Equation (20) is fulfilled.

$$D = \frac{\Delta H \cdot d_p \cdot rE_a}{h \cdot R_g \cdot T_g^2} < 0.3 \tag{20}$$

$\Delta H^{\circ}{}_{1023} = 2.61 \times 10^5$ J mol^{-1} (for methane dry reforming).Heat transfer coefficient (h) = 1192 W m^{-1} K^{-1} obtained from.Catalyst particle size diameter (d_p) = 250 μm = 250 $\times$ 10^{-6} m.Activation energy, E_a = 2.189 $\times$ 10^4 J mol^{-1}, (obtained from experimental result).R_g = 8.314 (universal gas constant).T_g = 1023 K (highest reaction temperature).

The highest experimental rate $(-r_{CO_2})$ is 1.36 $\times$ 10^{-8} mol g^{-1} s^{-1}, the reaction rate (r) per unit volume can be estimated as = 3.31 mol m^3 s^{-1} (measured bed density = 5.66 $\times$ 10^8 g m^{-3} and assume a very conservative bed voidage of 0.4). Substituting the

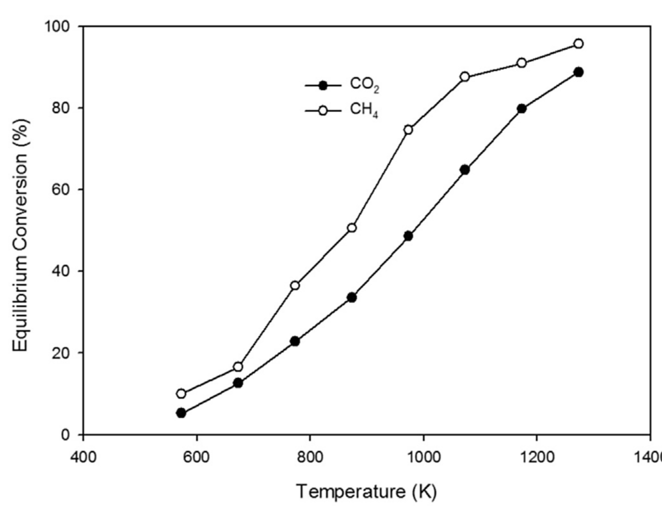

Fig. 11. Equilibrium conversions of CH_4 and CO_2 for methane dry reforming over 20 wt%Co/80 wt%Nd_2O_3 catalyst (P_{tot} = 101.3 kPa, CH_4:CO_2:1).

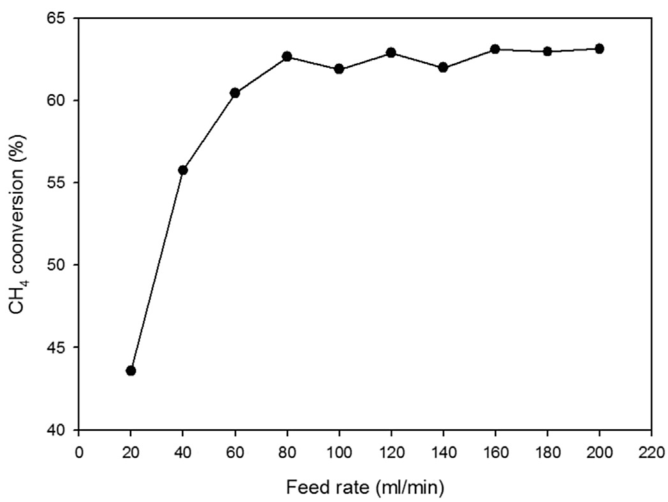

Fig. 12. Effect of feed rate on the conversion of CH_4 for methane dry reforming over 20 wt%Co/80 wt%Nd_2O_3 catalyst (reaction temperature = 1023 K, CH_4:CO_2:1).

above parameters in Equation (20) gives 4.56×10^{-4} which is less than 0.3. Hence, based on the Mears criterion, impact of external heat transfer on the kinetic measurement can be assumed negligible.

Based on the Weisz-Prater modulus criterion (Equation (21)) the impact of internal mass transfer on the kinetic measurement can be assumed negligible if the relationship in Equation (21) is meet.

$$D = \frac{r_{CO_2}\rho_s r_p^2 RT}{P_{CO_2} D_e} \le 1 \quad (21)$$

where r_{CO_2} is the observed highest rate of consumption $= 1.36 \times 10^{-8}\,\mathrm{mol\,g^{-1}\,s^{-1}} = 4.92 \times 10^{-5}\,\mathrm{mol\,g^{-1}\,h^{-1}}$.The Partial pressure of CO_2 at the external surface (P_{CO_2}) = 50.66×10^3 kPa = 0.566 atm Catalyst particle density (assumed spherical) $\rho_s = 0.956\,\mathrm{g\,m^{-3}}$,Radius of the catalyst particle (r_p), = 125×10^{-6} m.The mass transfer coefficient $D_e = 1.5 \times 10^{-6}\,\mathrm{m^2\,h^{-1}}$

Substituting these parameters in Equation (21), D value of 0.00145 is obtained which is less than 1. Hence, based on the Weisz-Prater modulus criterion, the impact of internal mass transfer on the reaction rate can be assumed negligible.

3.5. *Kinetic analysis*

3.5.1. *Effect of partial pressure*

The rate of consumption of CH_4 and CO_2 at temperature ranged 923–1023 K are depicted in Fig. 13. At constant CO_2 partial pressure the rate of consumption of CH_4 increases with CO_2 partial pressure and reaction temperature. Similarly, at constant CO_2 partial pressure the consumption rate of CH_4 also increases with increases with CH_4 partial pressure and temperature. In order to fully understand the behaviour of the methane dry reforming reaction over the 20 wt%Co/80 wt%Nd_2O_3 catalyst, the LH mechanism was proposed.

3.5.2. *Langmuir-Hinshelwood kinetic model*

Mechanistic studies of methane dry reforming have been reported based on the assumptions of Langmuir-Hinshelwood theoretical dual-site mechanisms (Ayodele et al., 2016b). Mechanisms steps such as dissociative adsorption of CH_4, molecular adsorption of CO_2 and carbon gasification by the adsorbed CO_2 on the basic site were considered. Based on these reported mechanistic studies, a sequence of mechanism steps for methane dry reforming over the current catalyst, 20 wt%Co/80 wt%Nd_2O_3 has been proposed, viz. (i) reversible adsorption and activation of CH_4 on the surface of the Co leading to the formation of H_2 and carbonaceous species (C), (ii) adsorption of CO_2 on the Nd_2O_3 basic site (ii) gasification of the C deposited on the Co surface by the lattice oxygen from the adsorbed CO_2. Rare earth metal oxide supports has been reported to have high oxygen storage capacity which produce mobile oxygen species on the surface of the catalyst (Sato et al., 2009). In addition, Fig. 14 illustrates the described mechanisms.

(i) Adsorption and activation of CH_4 on the (θ) provided by the cobalt

$$CH_4 + \theta \leftrightarrow \theta - CH_4 \quad (M1a)$$

$$\theta - CH_4 \leftrightarrow \theta - CH_3 + H \quad (M1b)$$

$$\theta - CH_3 \leftrightarrow \theta - CH_2 + H \quad (M1c)$$

$$\theta - CH_2 \leftrightarrow \theta - CH + H \quad (M1d)$$

$$\theta - CH \leftrightarrow \theta - C + H \quad (M1e)$$

In summary, the overall mechanistic step is:

$$\theta - CH_4 \leftrightarrow \theta - C + 2H_2\uparrow \quad (M1f)$$

(ii) Adsorption of CO_2 on basic (β) (Nd_2O_3) site

The adsorption of CO_2 on basic (β) (Nd_2O_3) site of the catalyst is evidenced by the formation of $Nd_2O_2CO_3$ shown in the XRD pattern of the used catalyst (cf.Fig. 4)

$$CO_2 + 2\beta \leftrightarrow \beta - CO_2 \quad (M2a)$$

$$\beta - CO_2 + O^{2-} \leftrightarrow \beta - CO_3^{2-} \quad (M2b)$$

whereby the O^{2-} was provided by the Nd_2O_3

(iii) Gasification of the carbon deposited on the surface of the Co

$$\beta - CO_3^{2-} + \theta - C \leftrightarrow \beta + \theta + 2CO\uparrow + O^{2-} \quad (M3)$$

Moreover, Langmuir-Hinshelwood kinetic model represented in Equation (22) was proposed based on the mechanisms in Equations (M1)–(M3), assuming that CH_4 and CO_2 adsorptions are at equilibrium, CH_4 activation by metal Co and C gasification by adsorbed CO_2 on the Nd_2O_3 support site are the rate determining steps (slow steps). The experimental data were fitted into Equation (20) to determine the kinetic parameters. Since Equation (20) is a non-linear model, the non-linear Levenberg-Marquardt regression package available in POLYMATH 6.1 software was employed to evaluate the kinetic parameters.

$$r_i = \frac{K_1 K_2 k_{CH_4} k_{CO_2} P_{CH_4} P_{CO_2}}{K_2 k_{CH_4} k_{CO_2} P_{CH_4} P_{CO_2} + K_1 K_2 k_{CH_4} P_{CH_4} + K_2 k_{CO_2} P_{CO_2}} \quad (22)$$

where r_i, K_1, K_2, k_{CH_4} and k_{CO_2} are the rate of consumption of the reaction species (CH_4 and CO_2), equilibrium constant of methane adsorption, equilibrium constant of CO_2 adsorption, equilibrium constant of CH_4 decomposition and equilibrium constant of reduction of CO_2 respectively.

The rate constant values, activation energy and the regression

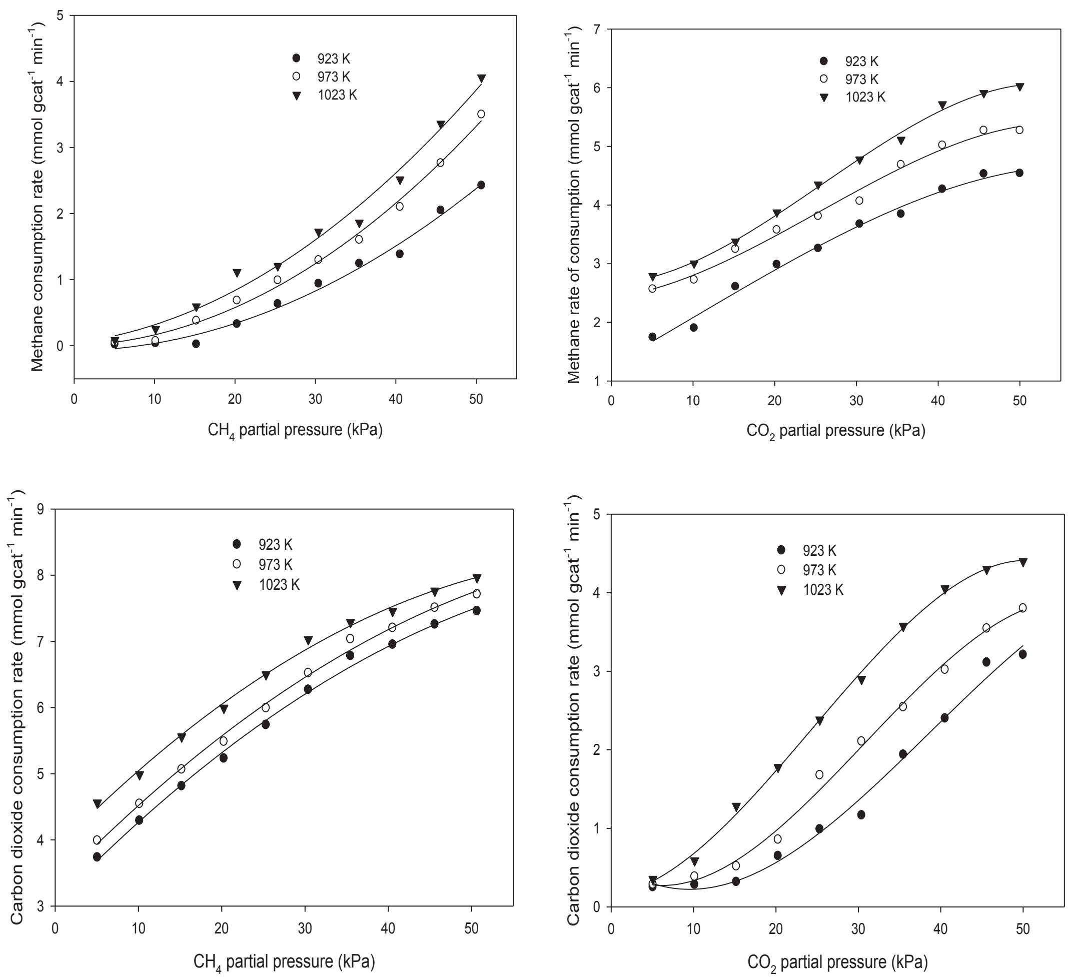

Fig. 13. The rate of consumption of methane and carbon dioxide as a function of temperature (a) varied CH_4 partial pressure at constant CO_2 partial pressure (b) varied CO_2 partial pressure at constant CH_4 partial pressure (c) varied CH_4 partial pressure at constant CO_2 partial pressure (d) varied CO_2 partial pressure at constant CH_4 partial pressure.

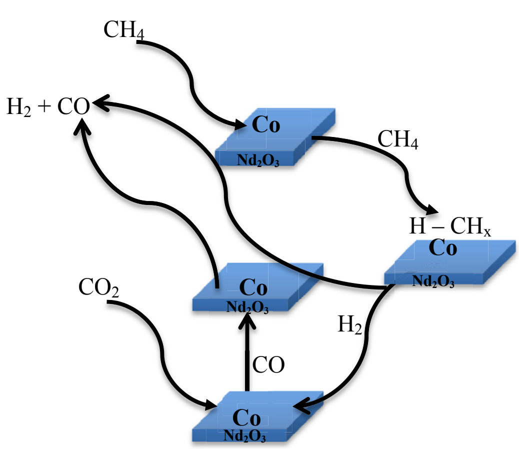

Fig. 14. Schematic diagram showing the mechanism of the catalytic reduction of the greenhouse gases over 20 wt%Co/80 wt%Nd_2O_3 catalyst.

Table 2
Langmuir-Hinshelwood kinetic model parameters.

Parameters	Temperature (K)		
	923	973	1023
K_1 (kPa^{-1})	6.59	7.44	8.88
E_{a1} (kJ mol^{-1})		23.38	
R^2		0.98	
K_2 (kPa^{-1})	5.37	6.96	7.47
E_{a2} (kJ mol^{-1})		26.16	
R^2		0.92	
k_{CH_4}(mol gcat^{-1} s^{-1})	1.43×10^{-2}	2.01×10^{-2}	3.16×10^{-2}
E_{CH_4}(kJ mol^{-1})		62.04	
R^2		0.98	
k_{CO_2}(mol gcat^{-1} s^{-1})	0.39	0.43	0.49
E_{CO_2} (kJ mol^{-1})		21.89	
R^2		0.96	

E_{a1} = apparent activation energy for CH_4 adsorption; E_{a2} = apparent activation energy for CO_2 adsorption.

coefficients estimated from the LH kinetic model are summarized in Table 2. The adsorption energy of 23.38 and 26.16 kJ mol^{-1} obtained for CH_4 and CO_2, respectively, showed that both CH_4 and CO_2 were chemically adsorbed onto the surface of the catalyst. Previous report (Munera et al., 2007) has shown that the adsorption energy of CH_4 was smaller compared to that of CO_2 which is consistent with our findings. Furthermore, the activation energy of 62.04 and 21.89 kJ mol^{-1} obtained for CH_4 and CO_2, respectively, was symptomatic of intrinsic chemical reaction and debunked any possibility of physical transport limitation that may have disguised the kinetics data. The apparent activation energy obtained for CH_4 in this

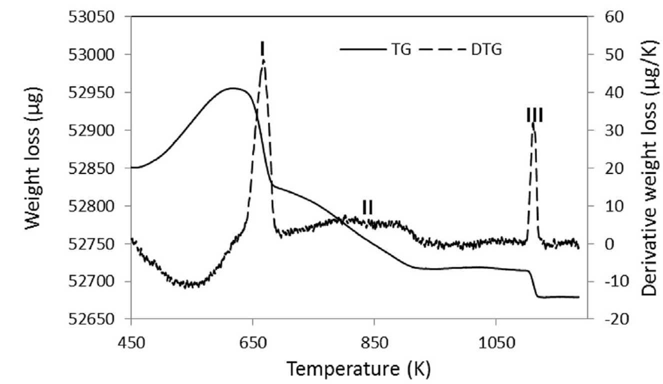

(a)

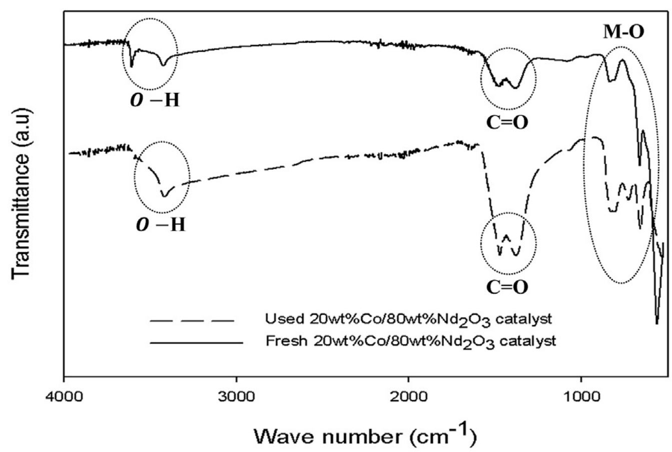

(b)

Fig. 15. (a) Temperature Programmed Oxidation and (b) FTIR spectra, of fresh and used 20 wt%Co/80 wt%Nd_2O_3 catalyst.

study is consistent with that reported by (Pichas et al., 2010) using CeO_2–Ni catalyst. Moreover, the lower value apparent activation energy obtained for CO_2 compared to CH_4 indicate rate of reaction of CO_2 proceeds faster compared to that of CH_4.

3.6. Characterization of the used 20 wt%Co/80 wt%Nd_2O_3 catalyst

One major constraint with heterogeneous catalytic reaction such as CO_2 reforming of methane is carbon deposition on the surface of the catalyst (Lee et al., 2014). The types of carbon deposition as well as the amount are function of the type of substrate (carbon source) and conditions of reaction (Arande et al., 1999). In the present study, the amount and type of carbon deposited on the surface of catalyst at 1023 K and GHSV of 30000 h^{-1} is presented as a representative sample. The resulting TPO profile is shown in Fig. 15(a). The influence of absorbed moisture which is usually detected at 373–400 K has been excluded from the TPO analysis. It is noteworthy that carbons are deposited on the surface of the catalyst used in the CO_2 reforming of methane. This is evident from the weight loss of the catalyst sample represented by peaks I-III (cf. Fig. 15(a)) as well as the XRD pattern of the used catalyst in Fig. 4. These could be attributed to oxidation of different carbon species deposited on the surface of the used catalyst (Wang et al., 2012). Interestingly, there was an initial increase in weight of the catalyst at temperature ranged 450–600 K. This could be attributed to the oxidation of the Co crystallite to CoO as previously reported by Foo et al. (2011) in their study on dry reforming of methane over alumina supported Co catalyst. Moreover, this implies carbon was deposited in the pores of the used catalyst rather than the surface. Furthermore, weight losses (peaks I-III) of the catalyst were observed at 650, 850 and 1110 K, respectively, representing different species of deposited carbon. Peak I (weight loss = 80 μg) can be attributed to oxidation of active or amorphous carbon, while peaks II (weight loss = 120 μg) and III (weight loss = 50 μg) can be attributed to the oxidation of graphite carbon (Son et al., 2014). The graphite carbon can either be whisky or encapsulating carbon. Based on literature reports, deposition of

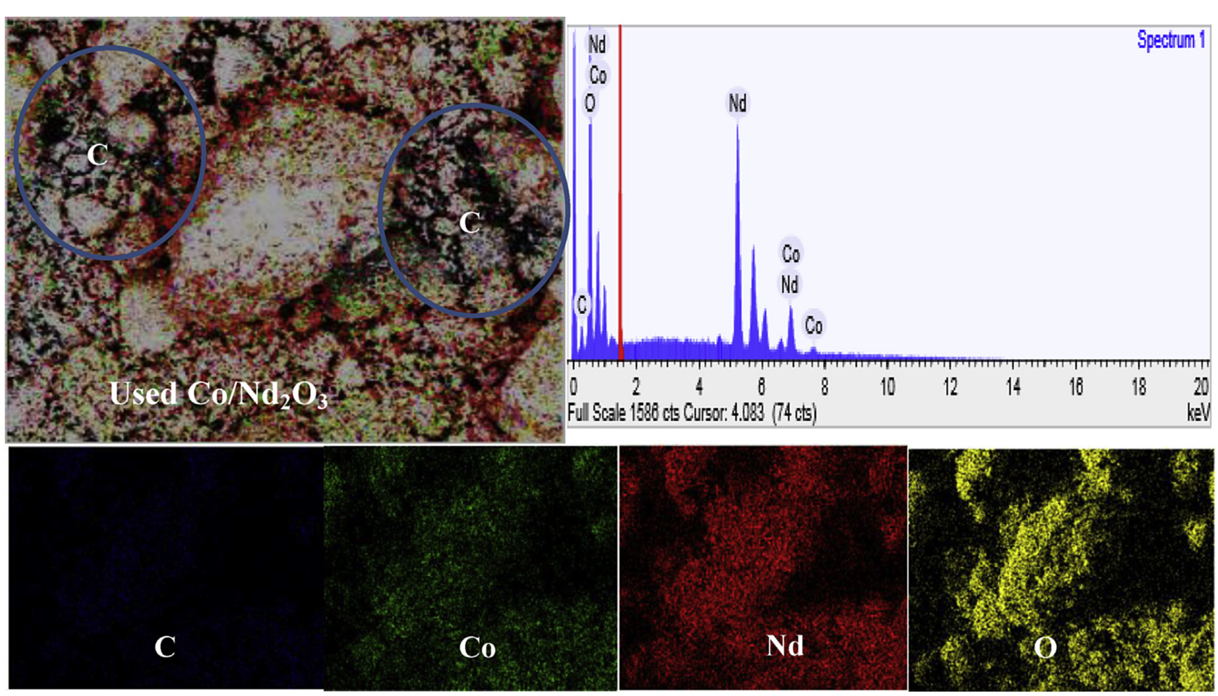

Fig. 16. EDX dot mapping and micrograph for the used 20 wt%Co/80 wt%Nd_2O_3 catalyst.

whisky carbons do not often result to catalyst deactivation but rather cause reactor blockage (Son et al., 2014). On the other hand, encapsulating carbons are mainly responsible for catalyst deactivation by encapsulating the active metal site with CH_x species (Bartholomew, 2001). Two major reactions namely Boudouard and methane decomposition have been reported to be the main sources of carbon deposition on the catalyst (Laosiripojana et al., 2005). Carbon formation from methane decomposition is favoured at high temperature since the decomposition process is endothermic (Horváth et al., 2011), while carbon formed from Boudouard reaction is favoured at low temperature due to its exothermic nature of the reaction (Lavoie, 2014).

In addition to the TPO analysis, the same used catalyst was further characterized by FTIR. The FTIR spectra of the fresh and used 20 wt%Co80 wt%Nd_2O_3 catalyst are shown in Fig. 15(b). The band around 500 and 790 cm^{-1} revealed the presence of bending and stretching M-O bond which could be attributed to Nd—O and Co—O, respectively. It can be seen that the stretching vibration M-O representing Co—O band present in the fresh catalyst at wave number ranged 500-790 cm^{-1} significantly reduced in the used catalyst leaving out the Nd—O bond. This further confirmed the possibility of carbon deposition on the catalyst which corroborated the TPO results for the used catalyst characterization. The existence of an extended C=O bond in the used catalyst at wave number ranged 1500 and 1364 cm^{-1} revealed the possibility of deposited carbon species on the used catalyst (Kępiński et al., 2004). The evidence of carbon is corroborated with the EDX dot mapping and micrograph shown in Fig. 16. The dark spots in the EDX dot mapping represent the carbon deposited on the surface of the used catalyst. The presence of the O—H bond at wave number ranged 3600–3400 cm^{-1} could be attributed to the presence of adsorbed moisture on the sample's surface prior to the FTIR analysis (Munera et al., 2007).

4. Conclusions

A 20 wt%Co/80 wt%Nd_2O_3 catalyst was synthesized and employed in catalytic CO_2 reforming of methane. Maximum CH_4 and CO_2 conversions of 62.7% and 82%, respectively, were obtained at feed ratio of 1.0 (highest ratio employed) and reaction temperature of 1023 K. Moreover, the production of syngas was observed to increase with feed ratio and temperature reaching the maximum product yield of 59.9% and 62.02% for H_2 and CO, respectively. In addition, the Langmuir-Hinshelwood theoretical dual-site mechanisms (based on the acquired NH_3- and CO_2-TPD analyses) modelling yielded activation energy of 62.04 and 21.89 kJ mol^{-1} for CH_4 and CO_2, respectively. The post-runs characterization of the 20 wt%Co/80wtNd_2O_3 catalyst using TPO, FTIR and SEM-EDX showed the presence of carbonaceous deposit. The evidence of carbon deposition on the surface of the used catalyst is an indication of the possible influence of side reactions such as reverse-Boudouard and reverse-water gas shift reactions during the CO_2 reforming of methane.

Acknowledgements

The authors would like to acknowledge the Sciencefund, RDU130501 granted by the Ministry of Science, Technology and Innovation Malaysia (MOSTI) and the prestigious DSS scholarship awarded to Bamidele Victor Ayodele by Universiti Malaysia Pahang. Osarieme U. Osazuwa thanks Institute of Postgraduate Studies, UMP for GRS scholarship.

References

Abasaeed, A.E., Al-fatesh, A.S., Naeem, M.A., Ibrahim, A.A., Fakeeha, A.H., 2015. Catalytic performance of CeO_2 and ZrO_2 supported Co catalysts for hydrogen production via dry reforming of methane. Int. Hydrog. Energy 6818–6826. http://dx.doi.org/10.1016/j.ijhydene.2015.03.152.

Acharya, C.K., Jiang, F., Liao, C.H., Fitzgerald, P., Vecchio, K.S., Cattolica, R.J., 2013. Tar and CO_2 removal from simulated producer gas with activated carbon and charcoal. Fuel Process. Technol. 106, 201–208. http://dx.doi.org/10.1016/j.fuproc.2012.07.026.

Arande, Josem M., Abajo, Inaki, Fernandez, Inmaculada, Lopez, Danilo, Javier, B., 1999. Kinetics of gaseous product formation in the coke combustion of a fluidized catalytic cracking catalyst. Ind. Eng. Chem. Res. 38, 3255–3260.

Ayodele, B.V., Khan, M.R., Cheng, C.K., 2015a. Catalytic performance of ceria-supported cobalt catalyst for CO-rich hydrogen production from dry reforming of methane. Int. J. Hydrogen Energy. http://dx.doi.org/10.1016/j.ijhydene.2015.10.049.

Ayodele, B.V., Khan, M.R., Cheng, C.K., 2015b. Syngas production from CO_2 reforming of methane over ceria supported cobalt catalyst: effects of reactants partial pressure. J. Nat. Gas. Sci. Eng. 27 (2), 1016–1023. http://dx.doi.org/10.1016/j.jngse.2015.09.049.

Ayodele, B.V., Hossain, M.A., Chong, S.L., Soh, J.C., Abdullah, S., Khan, M.R., Cheng, C.K., 2016a. Non-isothermal kinetics and mechanistic study of thermal decomposition of light rare earth metal nitrate hydrates using thermogravimetric analysis. J. Therm. Anal. Calorim. http://dx.doi.org/10.1007/s10973-016-5450-6.

Ayodele, B.V., Khan, M.R., Lam, S.S., Cheng, C.K., 2016b. Production of CO-rich hydrogen from methane dry reforming over lanthania-supported cobalt catalyst: kinetic and mechanistic studies. Int. J. Hydrogen Energy. http://dx.doi.org/10.1016/j.ijhydene.2016.01.091.

Ba, K., Oszk, A., Kecsk, T., Erd, A., 2014. Dry reforming of CH_4 on Rh doped Co/Al_2O_3 catalysts. Catal. Today 228, 123–130.

Bartholomew, C.H., 2001. Mechanisms of catalyst deactivation. Appl. Catal. A Gen. 212, 17–60. http://dx.doi.org/10.1016/S0926-860X(00)00843-7.

Blaine, R.L., Kissinger, H.E., 2012. Homer kissinger and the kissinger equation. Thermochim. Acta 540, 1–6. http://dx.doi.org/10.1016/j.tca.2012.04.008.

Botes, F.G., Niemantsverdriet, J.W., Van De Loosdrecht, J., 2013. A comparison of cobalt and iron based slurry phase Fischer-Tropsch synthesis. Catal. Today 215, 112–120. http://dx.doi.org/10.1016/j.cattod.2013.01.013.

Bouarab, R., Akdim, O., Auroux, A., Cherifi, O., Mirodatos, C., 2004. Effect of MgO additive on catalytic properties of Co/SiO_2 in the dry reforming of methane. Appl. Catal. A Gen. 264, 161–168. http://dx.doi.org/10.1016/j.apcata.2003.12.039.

Braga, T.P., Santos, R.C., Sales, B.M., da Silva, B.R., Pinheiro, A.N., Leite, E.R., Valentini, A., 2014. CO_2 mitigation by carbon nanotube formation during dry reforming of methane analyzed by factorial design combined with response surface methodology. Chin. J. Catal. 35, 514–523. http://dx.doi.org/10.1016/S1872-2067(14)60018-8.

Budiman, A.W., Song, S.H., Chang, T.S., Choi, M.J., 2016. Preparation of a high performance cobalt catalyst for CO_2 reforming of methane. Adv. Powder Technol. http://dx.doi.org/10.1016/j.apt.2016.01.029.

Choudhary, V.R., Mondal, K.C., 2006. CO_2 reforming of methane combined with steam reforming or partial oxidation of methane to syngas over $NdCoO_3$ perovskite-type mixed metal-oxide catalyst. Appl. Energy 83, 1024–1032. http://dx.doi.org/10.1016/j.apenergy.2005.09.008.

Clarke, L., Wise, M., Edmonds, J., Placet, M., Kyle, P., Calvin, K., Kim, S., Smith, S., 2009. CO_2 Emissions Mitigation and Technological Advance: An Updated Analysis of Advanced Technology Scenarios. Scenarios Updated January 2009.

Djinović, P., Batista, J., Pintar, A., 2012. Efficient catalytic abatement of greenhouse gases: methane reforming with CO_2 using a novel and thermally stable Rh-CeO_2 catalyst. Int. J. Hydrogen Energy 37, 2699–2707. http://dx.doi.org/10.1016/j.ijhydene.2011.10.107.

Donohue, M., Aranovich, G., 1998. Classification of Gibbs adsorption isotherms. Adv. Colloid Interface Sci. 76–77, 137–152. http://dx.doi.org/10.1016/S0001-8686(98)00044-X.

Ediger, V.Ş., Hoşgör, E., Sürmeli, a. N., Tatlıdil, H., 2007. Fossil fuel sustainability index: an application of resource management. Energy Policy 35, 2969–2977. http://dx.doi.org/10.1016/j.enpol.2006.10.011.

El Hassan, N., Kaydouh, M.N., Geagea, H., El Zein, H., Jabbour, K., Casale, S., El Zakhem, H., Massiani, P., 2016. Low temperature dry reforming of methane on rhodium and cobalt based catalysts: active phase stabilization by confinement in mesoporous SBA-15. Appl. Catal. A Gen. 520, 114–121. http://dx.doi.org/10.1016/j.apcata.2016.04.014.

Fakeeha, A.H., Naeem, M.A., Khan, W.U., Al-Fatesh, A.S., 2014. Syngas production via CO_2 reforming of methane using Co-Sr-Al catalyst. J. Ind. Eng. Chem. 20, 549–557. http://dx.doi.org/10.1016/j.jiec.2013.05.013.

Foo, S.Y., Cheng, C.K., Nguyen, T.-H., Adesina, A.a., 2011. Kinetic study of methane CO_2 reforming on Co—Ni/Al_2O_3 and Ce—Co—Ni/Al_2O_3 catalysts. Catal. Today 164, 221–226. http://dx.doi.org/10.1016/j.cattod.2010.10.092.

Giampietro, M., Mayumi, K., Ramos-Martin, J., 2006. Can biofuels replace fossil energy fuels? a multi-scale integrated analysis based on the concept of societal and ecosystem metabolism: Part 1. Int. J. Transdiscipl. Res. 1, 51–87.

Haag, S., Burgard, M., Ernst, B., 2007. Beneficial effects of the use of a nickel membrane reactor for the dry reforming of methane: comparison with thermodynamic predictions. J. Catal. 252, 190–204. http://dx.doi.org/10.1016/

j.jcat.2007.09.022.
Han, Y.K., Ahn, C., Bae, J., Kim, a R., Han, G.Y., 2013. Effects of carbon formation on catalytic performance for CO_2 reforming with methane on Ni/Al_2O_3 Catalyst: comparison of fixed- bed with fluidized-bed reactors. J. King Saud. Univ. Sci. 13288, 101–107.
Hashim, H., Ho, W., 2011. Renewable energy policies and initiatives for a sustainable energy future in Malaysia. Renew. Sustain. Energy Rev. 15, 4780–4787. http://dx.doi.org/10.1016/j.rser.2011.07.073.
Horváth, A., Stefler, G., Geszti, O., Kienneman, A., Pietraszek, A., Guczi, L., 2011. Methane dry reforming with CO_2 on CeZr-oxide supported Ni, NiRh and NiCo catalysts prepared by sol–gel technique: relationship between activity and coke formation. Catal. Today 169, 102–111. http://dx.doi.org/10.1016/j.cattod.2010.08.004.
Hussein, G.A.M., 1996. Rare earth metal oxides: formation, characterization and catalytic activity Thermoanalytical and applied pyrolysis review. J. Anal. Appl. Pyrolysis 37, 111–149. http://dx.doi.org/10.1016/0165-2370(96)00941-2.
Ihli, J., Wong, W.C., Noel, E.H., Kim, Y.-Y., Kulak, A.N., Christenson, H.K., Duer, M.J., Meldrum, F.C., 2014. Dehydration and crystallization of amorphous calcium carbonate in solution and in air. Nat. Commun. 5, 3169. http://dx.doi.org/10.1038/ncomms4169.
Itkulova, S.S., Zhunusova, K.S., Zakumbaeva, G., 2005. CO_2 reforming of methane over Co-Pd/Al_2O_3 catalysts. Bull. Korean Chem. Soc. 26, 2017–2020.
Jabbour, K., El Hassan, N., Casale, S., Estephane, J., El Zakhem, H., 2014. Promotional effect of Ru on the activity and stability of Co/SBA-15 catalysts in dry reforming of methane. Int. J. Hydrogen Energy 39, 7780–7787. http://dx.doi.org/10.1016/j.ijhydene.2014.03.040.
Jacobs, G., Das, T.K., Zhang, Y., Li, J., Racoillet, G., Davis, B.H., 2002. Fischer–Tropsch synthesis: support, loading, and promoter effects on the reducibility of cobalt catalysts. Appl. Catal. A Gen. 233, 263–281. http://dx.doi.org/10.1016/S0926-860X(02)00195-3.
Khodakov, A.Y., Chu, W., Fongarland, P., 2007. Advances in the development of novel cobalt fischer – tropsch catalysts for synthesis of long-chain hydrocarbons and clean fuels advances in the development of novel cobalt fischer – tropsch catalysts for synthesis of long-chain hydrocarbons and clean fue. Chem. Rev. 107, 1692–1744. http://dx.doi.org/10.1021/cr050972v.
Kępiński, L., Zawadzki, M., Miśta, W., 2004. Hydrothermal synthesis of precursors of neodymium oxide nanoparticles. Solid State Sci. 6, 1327–1336. http://dx.doi.org/10.1016/j.solidstatesciences.2004.07.003.
Lakhapatri, S.L., Abraham, M.A., 2009. Deactivation due to sulfur poisoning and carbon deposition on Rh-Ni/Al_2O_3 catalyst during steam reforming of sulfur-doped n-hexadecane. Appl. Catal. A Gen. 364, 113–121. http://dx.doi.org/10.1016/j.apcata.2009.05.035.
Laosiripojana, N., Sutthisripok, W., Assabumrungrat, S., 2005. Synthesis gas production from dry reforming of methane over CeO_2 doped Ni/Al_2O_3: influence of the doping ceria on the resistance toward carbon formation. Chem. Eng. J. 112, 13–22. http://dx.doi.org/10.1016/j.cej.2005.06.003.
Lavoie, J.-M., 2014. Review on dry reforming of methane, a potentially more environmentally-friendly approach to the increasing natural gas exploitation. Front. Chem. 2, 1–17. http://dx.doi.org/10.3389/fchem.2014.00081.
Lee, J.-H., You, Y.-W., Ahn, H.-C., Hong, J.-S., Kim, S.-B., Chang, T.-S., Suh, J.-K., 2014. The deactivation study of Co–Ru–Zr catalyst depending on supports in the dry reforming of carbon dioxide. J. Ind. Eng. Chem. 20, 284–289. http://dx.doi.org/10.1016/j.jiec.2013.03.036.
Ma, W.P., Ding, Y.J., Lin, L.W., 2004. Fischer-Tropsch synthesis over activated-carbon-supported cobalt catalysts: effect of Co loading and promoters on catalyst performance. Ind. Eng. Chem. Res. 43, 2391–2398. http://dx.doi.org/10.1021/Ie034116q.
Mattos, L.V., Rodino, E., Resasco, D.E., Passos, F.B., Noronha, F.B., 2003. Partial oxidation and CO_2 reforming of methane on Pt/Al_2O_3, Pt/ZrO_2, and Pt/Ce-ZrO_2 catalysts. Fuel Process. Technol. 83, 147–161. http://dx.doi.org/10.1016/S0378-3820(03)00063-8.
Mears, D.E., 1971. Tests for transport limitations in experimental catalytic reactors. Ind. Eng. Chem. Process Des. Dev. 10, 541–547. http://dx.doi.org/10.1021/i260040a020.
Moore, C.W., Zielinska, B., Pétron, G., Jackson, R.B., 2014. Air impacts of increased natural gas acquisition, processing, and use: a critical review. Environ. Sci. Technol. 48, 8349–8359. http://dx.doi.org/10.1021/es4053472.
Munera, J., Irusta, S., Cornaglia, L., Lombardo, E., Vargascesar, D., Schmal, M., 2007. Kinetics and reaction pathway of the CO_2 reforming of methane on Rh supported on lanthanum-based solid. J. Catal. 245, 25–34. http://dx.doi.org/10.1016/j.jcat.2006.09.008.
Nair, M.M., Kaliaguine, S., Kleitz, F., 2014. Nanocast $LaNiO_3$ perovskites as precursors for the preparation of coke-resistant dry reforming catalysts. ACS Catal. 4, 3837–3846.
Nematollahi, B., Rezaei, M., Khajenoori, M., 2011. Combined dry reforming and partial oxidation of methane to synthesis gas on noble metal catalysts. Int. J. Hydrogen Energy 36, 2969–2978. http://dx.doi.org/10.1016/j.ijhydene.2010.12.007.
Ocsachoque, M., Pompeo, F., Gonzalez, G., 2011. Rh–Ni/CeO_2–Al_2O_3 catalysts for methane dry reforming. Catal. Today 172, 226–231. http://dx.doi.org/10.1016/j.cattod.2011.02.057.
Pakhare, D., Schwartz, V., Abdelsayed, V., Haynes, D., Shekhawat, D., Poston, J., Spivey, J., 2014. Kinetic and mechanistic study of dry (CO_2) reforming of methane over Rh-substituted La2Zr2O7 pyrochlores. J. Catal. 316, 78–92. http://dx.doi.org/10.1016/j.jcat.2014.04.023.
Peleg, M., Normand, M.D., Corradini, M.G., 2012. The Arrhenius equation revisited. Crit. Rev. Food Sci. Nutr. 52, 830–851.
British Petroleum, 2013. BP Statistical Review of World Energy. BPstats. http://scholar.google.com/scholar?hl=en&btnG=Search&q=intitle:BP+Statistical+Review+of+World+Energy#0.
Pichas, C., Pomonis, P., Petrakis, D., Ladavos, A., 2010. Kinetic study of the catalytic dry reforming of CH_4 with CO_2 over $La_{2-x}Sr_xNiO_4$ perovskite-type oxides. Appl. Catal. A Gen. 386, 116–123. http://dx.doi.org/10.1016/j.apcata.2010.07.043.
Rabelo, S.C., Carrere, H., Maciel Filho, R., Costa, a.C., 2011. Production of bioethanol, methane and heat from sugarcane bagasse in a biorefinery concept. Bioresour. Technol. 102, 7887–7895. http://dx.doi.org/10.1016/j.biortech.2011.05.081.
Ramírez-Verduzco, L., 2012. Predicting cetane number, kinematic viscosity, density and higher heating value of biodiesel from its fatty acid methyl ester composition. Fuel 91, 102–111. http://dx.doi.org/10.1016/j.fuel.2011.06.070.
Ross, J.R.H., 2005. Natural gas reforming and CO_2 mitigation. Catal. Today 100, 151–158. http://dx.doi.org/10.1016/j.cattod.2005.03.044.
Ruckenstein, E., Wang, H., 2000. Carbon dioxide reforming of methane to synthesis gas over supported cobalt catalysts. Appl. Catal. A Gen. 204, 257–263. http://dx.doi.org/10.1016/S0926-860X(00)00674-8.
Sajjadi, S.M., Haghighi, M., Rahmani, F., 2014. Dry reforming of greenhouse gases CH_4/CO_2 over MgO-promoted Ni-Co/Al_2O_3-ZrO_2 nanocatalyst: effect of MgO addition via sol-gel method on catalytic properties and hydrogen yield. J. Sol-Gel Sci. Technol. 1–14. http://dx.doi.org/10.1007/s10971-014-3280-1.
Sato, K., Fujimoto, K., 2007. Development of new nickel based catalyst for tar reforming with superior resistance to sulfur poisoning and coking in biomass gasification. Catal. Commun. 8, 1697–1701. http://dx.doi.org/10.1016/j.catcom.2007.01.028.
Sato, S., Takahashi, R., Kobune, M., Gotoh, H., 2009. Basic properties of rare earth oxides. Appl. Catal. A Gen. 356, 57–63. http://dx.doi.org/10.1016/j.apcata.2008.12.019.
Serrano-Lotina, A., Daza, L., 2014. Influence of the operating parameters over dry reforming of methane to syngas. Int. J. Hydrogen Energy 39, 4089–4094. http://dx.doi.org/10.1016/j.ijhydene.2013.05.135.
Shafiee, S., Topal, E., 2009. When will fossil fuel reserves be diminished? Energy Policy 37, 181–189. http://dx.doi.org/10.1016/j.enpol.2008.08.016.
Shearer, C., Bistline, J., Inman, M., Davis, S.J., 2014. The effect of natural gas supply on US renewable energy and CO_2 emissions. Environ. Res. Lett. 9, 094008. http://dx.doi.org/10.1088/1748-9326/9/9/094008.
Sokolov, S., Kondratenko, E.V., Pohl, M.-M., Rodemerck, U., 2013. Effect of calcination conditions on time on-stream performance of Ni/La_2O_3–ZrO_2 in low-temperature dry reforming of methane. Int. J. Hydrogen Energy 38, 16121–16132. http://dx.doi.org/10.1016/j.ijhydene.2013.10.013.
Son, I.H., Lee, S.J., Song, I.Y., Jeon, W.S., Jung, I., Yun, D.J., Jeong, D.-W., Shim, J.-O., Jang, W.-J., Roh, H.-S., 2014. Study on coke formation over Ni/γ-Al_2O_3, Co-Ni/γ-Al_2O_3, and Mg-Co-Ni/γ-Al_2O_3 catalysts for carbon dioxide reforming of methane. Fuel 136, 194–200. http://dx.doi.org/10.1016/j.fuel.2014.07.041.
Takanabe, K., Nagaoka, K., Nariai, K., Aika, K., 2005. Influence of reduction temperature on the catalytic behavior of Co/TiO_2 catalysts for CH_4/CO_2 reforming and its relation with titania bulk crystal structure. J. Catal. 230, 75–85. http://dx.doi.org/10.1016/j.jcat.2004.11.005.
Timko, M.T., Herndon, S.C., de la Rosa Blanco, E., Wood, E.C., Yu, Z., Miake-Lye, R.C., Knighton, W.B., Shafer, L., DeWitt, M.J., Corporan, E., 2011. Combustion products of Petroleum jet fuel, a fischer–tropsch synthetic fuel, and a biomass fatty acid methyl ester fuel for a gas turbine engine. Combust. Sci. Technol. 183, 1039–1068. http://dx.doi.org/10.1080/00102202.2011.581717.
Tungkamani, S., Phongaksorn, M., 2013. Developing Carbon Tolerance Catalyst for Dry Methane Reforming 32, pp. 745–750.
Union gas, 2015. Chemical Composition of Natural Gas-Union Gas Chemical Composition of Natural Gas Chemical Composition of Natural Gas-Union Gas [WWW Document]. A Spectr. Energy Co. www.uniongas.com.
Verykios, X.E., 2003. Catalytic dry reforming of natural gas for the production of chemicals and hydrogen. Int. J. Hydrogen Energy 28, 1045–1063. http://dx.doi.org/10.1016/S0360-3199(02)00215-X.
Wang, N., Chu, W., Zhang, T., Zhao, X.S., 2012. Synthesis, characterization and catalytic performances of Ce-SBA-15 supported nickel catalysts for methane dry reforming to hydrogen and syngas. Int. J. Hydrogen Energy 37, 19–30. http://dx.doi.org/10.1016/j.ijhydene.2011.03.138.
Weisz, P.B., Prater, C.D., 1954. Interpretation of measurements in experimental catalysis. Adv. Catal. 6, 143–196. http://dx.doi.org/10.1016/S0360-0564(08)60390-9.
Zhang, B., Tang, X., Li, Y., Cai, W., Xu, Y., Shen, W., 2006. Steam reforming of bio-ethanol for the production of hydrogen over ceria-supported Co, Ir and Ni catalysts. Catal. Commun. 7, 367–372. http://dx.doi.org/10.1016/j.catcom.2005.12.014.
Zhang, J., Wang, H., Dalai, a, 2007. Development of stable bimetallic catalysts for carbon dioxide reforming of methane. J. Catal. 249, 300–310. http://dx.doi.org/10.1016/j.jcat.2007.05.004.